Electrical characterization of transparent $p-i-n$ heterojunction diodes

R. L. Hoffman and J. F. Wager[a)]
Department of Electrical and Computer Engineering, Oregon State University, Corvallis, Oregon 97331-3211

M. K. Jayaraj and J. Tate
Department of Physics, Oregon State University, Corvallis, Oregon 97331

(Received 19 June 2001; accepted for publication 28 August 2001)

Transparent $p-i-n$ heterojunction diodes are fabricated using heavily doped, *p*-type $CuYO_2$ and semi-insulating *i*-ZnO thin films deposited onto a glass substrate coated with *n*-type indium tin oxide. Rectification is observed, with a ratio of forward-to-reverse current as high as 60 in the range $-4-4$ V. The forward-bias current–voltage characteristics are dominated by the flow of space-charge-limited current, which is ascribed to single-carrier injection into the *i*-ZnO layer. Capacitance measurements show strong frequency dispersion, which is attributed to *i*-ZnO traps. The diode structure has a total thickness of 0.75 μm and an optical transmission of ~35%–65% in the visible region. © *2001 American Institute of Physics.* [DOI: 10.1063/1.1413710]

I. INTRODUCTION

The report of *p*-type conductivity in transparent $CuAlO_2$ films[1] has attracted much attention, since in conjunction with *n*-type transparent conducting oxides such as ZnO they provide a route for the realization of transparent electronic and optoelectronic devices. Several similar compounds having the delafossite structure of $CuAlO_2$ have been reported recently with varying conductivity and transparency.[2–5] Increasingly conductive *p*-type delafossite thin films of $CuYO_2$:Ca,[3] $CuScO_2$,[2] and $CuCrO_2$:Mg,[4] with conductivities of 1, 30, and 220 S cm^{-1}, respectively, have been realized. All-oxide transparent $p-n$ junctions and light-emitting diodes have been successfully fabricated using ZnO and $SrCu_2O_2$.[6,7] Rectifying behavior in other oxide structures has also been reported, including *p*-NiO/*i*-NiO/*i*-ZnO/*n*-ZnO (Ref. 8) and *n*-ZnO/*p*-ZnO,[9] although well-characterized *p*-type ZnO has proven elusive. Bipolarity has been reported in the $CuInO_2$ delafossite system, with the promise of a transparent oxide $p-n$ homojunction.[10]

The purpose of this article is to report on the electrical characteristics of all-oxide transparent $p-i-n$ heterojunction diodes fabricated using $CuYO_2$:Ca as the *p*-type transparent conductive oxide.

II. DEVICE FABRICATION AND MATERIALS CHARACTERIZATION

Transparent $p-i-n$ heterojunction diodes have the structure *p*-$CuYO_2$:Ca/*i*-ZnO/*n*-indium tin oxide (ITO)/glass, as shown in Fig. 1.[11] The 1 in. glass substrate, coated with a 200 nm sputtered ITO film, is supplied by Planar Systems. ITO is highly transparent (>85% in the visible region) and has a conductivity in the range 10^3-10^4 S cm^{-1}. ZnO is deposited onto the ITO-coated glass by rf magnetron sputtering at a substrate temperature of 150 °C, 10 mTorr of pure Ar as the sputtering gas, target-to-substrate distance of 2.5 cm, and rf power of 100 W; the film thickness is ~250 nm. Two doping procedures are employed to vary the carrier concentration in the ZnO films; heavily doped n^+-ZnO:Al is sputtered from a ZnO target doped with 2% Al; undoped, nonstoichiometric n-ZnO_{1-y} from a pure ZnO target. *P*-type $CuYO_2$:Ca is deposited through a shadow mask at a substrate temperature of 100 °C by reactive co-evaporation. Y, Cu, and Ca are thermally evaporated from refractory boats at a working molecular oxygen pressure of 150 μTorr. The thickness of the $CuYO_2$:Ca layer is ~300 nm. After deposition of the *p*-type layer, the device is subjected to a rapid thermal anneal (RTA) for 3 min at 600 °C in oxygen. This RTA process improves the conductivity of the *p*-type $CuYO_2$:Ca via O intercalation, but also renders the ZnO layer semi-insulating ($\sigma<0.1$ S cm^{-1}); this is at least partially attributable to the annihilation of oxygen vacancies, which act as donors in ZnO. Finally, In is used to make Ohmic contact to the $CuYO_2$:Ca and ITO layers.

Hall-mobility and conductivity measurements are performed using the van der Pauw configuration. For ZnO:Al, the Hall mobility $\mu=11.9$ cm^2 V^{-1} s^{-1} and conductivity $\sigma=1800$ S cm^{-1} give a carrier concentration $n=9.6\times10^{20}$ cm^{-3}. For an undoped, nonstoichiometric ZnO film, the Hall mobility $\mu=6.2$ cm^2 V^{-1} s^{-1} and conductivity $\sigma=50$ S cm^{-1} give a carrier concentration $n=5\times10^{19}$ cm^{-3}. These measurements are for ZnO films sputtered on glass, with no postdeposition annealing; both types of ZnO are strongly affected by the high-temperature oxygen anneal required for the $CuYO_2$:Ca layer.

The $CuYO_2$:Ca films show *p*-type conductivity by thermoelectric probe measurements, with a Seebeck coefficient of 280 μV K^{-1}. Hall measurements could not determine the mobility of holes in the $CuYO_2$ films, thus placing an approximate upper limit on mobility of ~1 cm^2 V^{-1} s^{-1}. Using this mobility value results in a minimum carrier concentration of $p\sim1\times10^{19}$ cm^{-3} for *p*-type $CuYO_2$:Ca. $CuYO_2$:Ca thin films typically exhibit ~40%–50% transparency in the visible region of the electromagnetic spectrum.

a)Electronic mail: jfw@ece.orst.edu

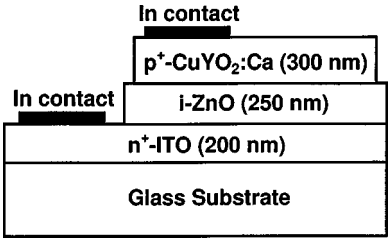

FIG. 1. Structure of the $CuYO_2$:Ca/ZnO/ITO $p-i-n$ heterojunction diode.

III. DEVICE CHARACTERIZATION

A. Energy-band considerations

An approximate equilibrium energy-band diagram for the transparent $CuYO_2$:Ca/ZnO/ITO $p-i-n$ heterojunction diode is shown in Fig. 2. ITO is *n* type, has a band gap of ~ 3.6 eV,[12] and is degenerately doped, so that its Fermi level, E_F, is positioned slightly above the conduction-band minimum, E_C. The ZnO band gap is ~ 3.3 eV.[13] As mentioned previously, the ZnO layer becomes semi-insulating ($\sigma < \sim 0.1$)S cm^{-1} after the 600 °C RTA treatment in oxygen, corresponding to an electron concentration, $n \leqslant \sim 10^{17}$ cm^{-3}, which is at least two orders of magnitude smaller than the carrier concentration of the $CuYO_2$:Ca or the ITO layers.

Sketching the $CuYO_2$:Ca portion of the energy-band diagram shown in Fig. 2 is more difficult since there is some uncertainty regarding the band gap of $CuYO_2$. Figure 3 shows $(\alpha h\nu)^{1/2}$ and $(\alpha h\nu)^2$ plots of the absorption edge of an undoped $CuYO_2$ thin film for estimation of the indirect and direct allowed optical band gaps, respectively. This results in estimates of ~ 1.2 and ~ 3.6 eV for indirect and direct band gaps, respectively, in agreement with those reported by Benko and Koffyberg for Ca-doped $CuYO_2$, from photoelectrochemical measurements.[14] These band-gap identifications are consistent with the optoelectronic assessment and electronic structure calculations of Yanagi *et al.* who find for $CuAlO_2$, a similar delafossite material, an indirect band gap at ~ 1.8 eV and a direct band gap at ~ 3.5 eV.[15]

However, these conclusions are inconsistent with an electronic structure calculation of Mattheis, who asserts the $CuYO_2$ minimum band gap to be direct at ~ 2.7 eV and finds that interstitial oxygen doping results in the evolution of midgap impurity bands, thus decreasing the effective band gap.[16] Additionally, from soft x-ray photoabsorption spectroscopy measurements, Cava *et al.* observe the emergence of new unoccupied band-gap states as they oxygen dope $CuYO_2$ to obtain $CuYO_{2.55}$.[17] They interpret their measurements as indicating that Cu atoms in $CuYO_2$ are in the Cu^{1+} oxidation state, characterized by a $2p^6 3d^{10} \rightarrow 2p^5 3d^{10} 4s^1$ photoabsorption transition, but that oxidized Cu atoms in $CuYO_{2.55}$ are in the Cu^{2+} oxidation state, characterized by a $2p^6 3d^9 \rightarrow 2p^5 3d^{10}$ photoabsorption transition. Thus, the results of Mattheis and Cava *et al.* suggest that the ~ 1.2 eV indirect band gap estimated from optical absorption measurements could be an extrinsic effect arising from oxygen intercalation doping which, in fact, we employ to improve the conductivity of our $CuYO_2$ layers. Furthermore, assume that $CuYO_2$ is indeed a wide-band-gap material, with a minimum band gap corresponding to Mattheis' underestimated (by his own admission) calculated ~ 2.7 eV direct band gap or Benko and Koffyberg and our measured ~ 3.6 eV direct band gap. It is likely that oxygen intercalation doping, substitutional doping (e.g., Ca doping), or unintentional impurity incorporation would indirectly give rise to new and probably deep states in the gap via self-compensation,[18] in addition to the band-gap states produced directly from the incorporation of these dopants/impurities. Such directly and indirectly produced gap states would result in a decrease in the effective band gap as estimated from optical absorption measurements.

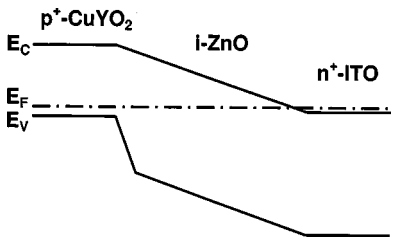

FIG. 2. Equilibrium energy band diagram for a $CuYO_2$:Ca/ZnO/ITO $p-i-n$ heterojunction diode.

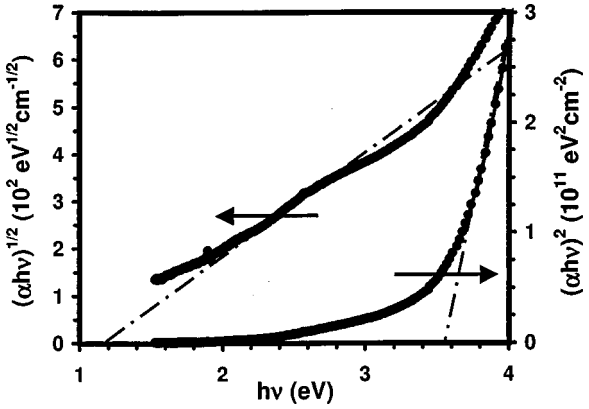

FIG. 3. $(\alpha h\nu)^{1/2}$ and $(\alpha h\nu)^2$ plots of the absorption edge of an undoped $CuYO_2$ thin film for estimation of the indirect and direct allowed optical band gaps, respectively. This results in an indirect band gap of ~ 1.2 and a direct band gap of ~ 3.6 eV.

Returning to Fig. 3, our appraisal of the literature indicates that the strong absorption edge at ~ 3.6 eV corresponds to an allowed direct band gap. The origin of the weak absorption edge at ~ 1.2 eV is less certain. Most likely it corresponds to absorption associated with either an intrinsic, indirect band gap or some type of extrinsic doping, impurity incorporation, or self-compensation-induced gap states. More work is required to unequivocally establish which absorption mechanism is operative. Regardless of the absorption mechanism, we regard this omnipresent weak absorption edge as evidence that the band gap or effective band gap which establishes the $p-i-n$ diode electronic properties is approximately ~ 1.2 eV. Moreover, the Fermi level must be positioned near the valence band maximum since the hole concentration is so large. This energy-band situation is indicated in Fig. 2.

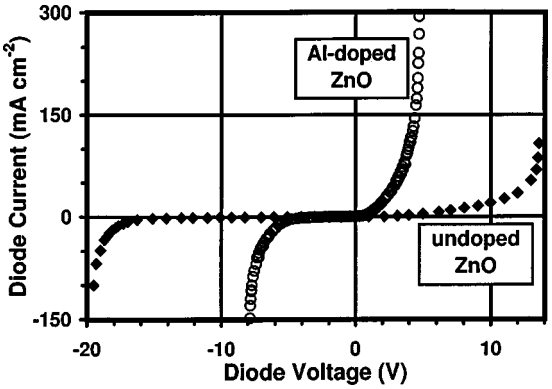

FIG. 4. I–V characteristics for two types of $CuYO_2$:Ca/ZnO/ITO p–i–n heterojunction diodes in which the ZnO layer is either undoped or doped with Al.

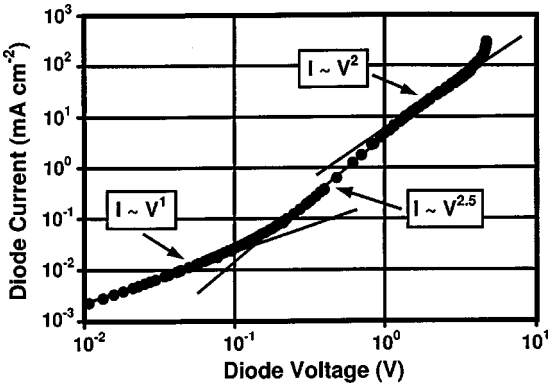

FIG. 6. Forward-bias log(I)–log(V) characteristics of a $CuYO_2$:Ca/ZnO/ITO p–i–n heterojunction diode in which the ZnO layer is Al doped. Three power law fits to different portions of the log(I)–log(V) curve are shown.

Two aspects of Fig. 2 merit further comment. First, the high-temperature RTA treatment employed to fabricate these p–i–n heterojunctions very likely results in interdiffusion and compositionally graded, rather than abrupt, interfaces. Such compositional grading precludes interfacial conduction- or valence-band discontinuities and results in a smooth transition between bulk energy bands. Second, due to the significant mismatch in band gaps between $CuYO_2$ and ZnO, the barrier for hole injection at the p–i interface is $\sim$2.1 eV larger than the barrier for injection of electrons at the n–i interface. This suggests that the forward bias current is likely to be essentially unipolar, due predominantly to the injection of electrons from ITO. This unipolar behavior is a departure from normal p–i–n homojunction diode behavior, where bipolar carrier injection and recombination in the i layer is the dominant current mechanism.[19]

B. Current–voltage characteristics

Figure 4 presents typical I–V curves for two types of $CuYO_2$:Ca/ZnO/ITO p–i–n heterojunction diode in which the ZnO layer is either undoped or doped with Al. Figures 5 and 6 display corresponding forward bias ln(I)–V and log(I)–log(V) curves for the ZnO:Al device. Several features of these I–V characteristics are noteworthy.

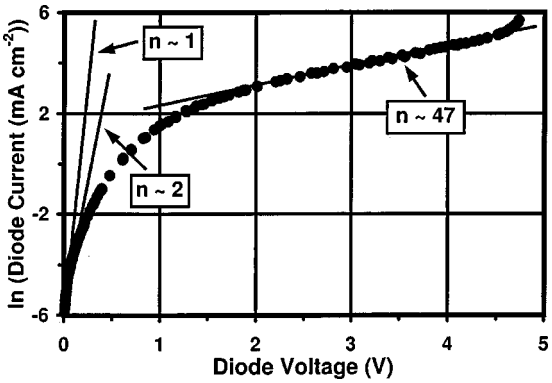

FIG. 5. Forward-bias ln(I)–V characteristics of a $CuYO_2$:Ca/ZnO/ITO p–i–n heterojunction diode in which the ZnO layer is Al doped. Exponential fit lines correspond to ideality factors $n=1$, 2, and 47.

First, these diodes clearly exhibit rectification. A maximum forward-to-reverse current ratio of 60 occurs at ± 4 V for the ZnO:Al structure, and at ± 5 V for the structure containing undoped ZnO. In reverse bias, the initially small leakage current is followed by a rather soft breakdown. Both diode structures are able to sustain a maximum current of 10 mA (150 mA cm^{-2}) or more in both forward and reverse bias.

Second, Figs. 4 and 6 provide evidence that the series resistance of these devices is small and does not make a significant contribution to the measured I–V curve trend. An upper bound for the series resistance may be estimated from Fig. 4 as the inverse of the slope of the I–V curve at the largest forward bias; the maximum series resistance estimated in this manner is $\sim 25\ \Omega$ for these diodes. Additional evidence that the series resistance actually must be smaller than this estimate is available from Fig. 6, when it is recognized that a log(I)–log(V) curve should give rise to a $I \propto V^1$ power law at large forward bias if the diode is series-resistance limited; Fig. 6 clearly shows that this is not the case.

Third, Fig. 5 shows that the diode does not conform to the ''normal'' forward-bias I–V relationship in which the current depends exponentially on the voltage divided by a product of the thermal energy times an ideality factor of $n=1$ or 2.[19] An illustration of the futility of trying to fit a typical measured ln(I)–V curve with $n=1$ or 2 is shown in Fig. 5. Observe that a significant portion of the ln(I)–V curve can be well fit using $n=47$; an n of such a large magnitude argues against the viability of employing an exponential relationship to account for this I–V trend.

The power-law fits shown in Fig. 6 provide insight into the operative mechanisms responsible for the I–V trends of $CuYO_2$:Ca/ZnO/ITO p–i–n heterojunction diodes. At very small voltages, $I \propto V^1$, indicating that Ohmic conduction prevails. At larger voltages, $I \propto V^2$, corresponding to a shallow-trap square-law regime, characteristic of space-charge-limited current (SCLC).[20] At intermediate voltages, $I \propto V^{2.5}$, corresponding to a transition between Ohmic and classical SCLC; transition regions such as this often arise in SCLC-dominated I–V characteristics and are attributed to the presence of traps near the Fermi level of the layer in which

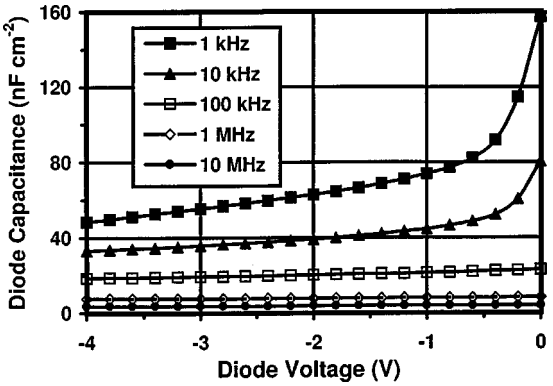

FIG. 7. Reverse-bias $C-V$ characteristics of a $CuYO_2$:Ca/ZnO:Al/ITO $p-i-n$ heterojunction diode obtained at frequencies of 1 kHz, 10 kHz, 100 kHz, 1 MHz, and 10 MHz.

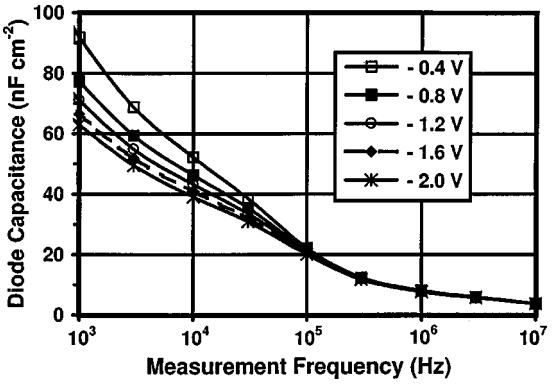

FIG. 8. Reverse-bias $C-f$ characteristics of a $CuYO_2$:Ca/ZnO:Al/ITO $p-i-n$ heterojunction diode for reverse biases of -0.4, -0.8, -1.2, -1.6, and -2.0 V.

SCLC flow occurs (e.g., see Fig. 4.5 of Ref. 20). Finally, at the largest applied forward biases, the log(I)–log(V) curve deviates from a square-law dependence, bending upward with a much greater slope; this regime is likely due to the onset of a trap-filled limit (TFL), double injection, or (less likely) breakdown.

A bit of deconstruction of the last paragraph is perhaps warranted. Ideal SCLC is observed when carriers are injected from contacts into a perfect insulator. Since the ideal insulator contains no free carriers in equilibrium, these injected carriers establish space charge in the insulator bulk. Further carrier injection is inhibited by the presence of this injected space charge, giving rise to $I \propto V^2$ square-law characteristics. In practice, some free carriers are present in equilibrium so that ohmic conduction dominates the $I-V$ characteristics at the smallest applied voltages. Also, because of nonidealities such as bulk trapping of injected carriers and various possible bulk trap distributions, SCLC behavior is often found to be proportional to a power of the applied voltage greater than 2, as observed in the transition region of the log(I)–log(V) curve shown in Fig. 6 in which $I \propto V^{2.5}$.

C. Capacitance characteristics

Figure 7 presents capacitance–voltage ($C-V$) characteristics at selected discrete measurement frequencies between 1 kHz and 10 MHz. Figure 8 shows the measured capacitance–frequency ($C-f$) characteristics at reverse biases from 0.4 to 2.0 V. Capacitance measurements shown here are for an Al-doped ZnO device, but are typical of capacitance measurements for both undoped and Al-doped ZnO devices.

The capacitance of a trap-free diode is expected to decrease with increasing reverse bias, due to an increase in the depletion region width, and to be independent of the measurement signal frequency. Thus, the voltage dependence of the 1 and 10 kHz curves shown in Fig. 7 is consistent with the expected trend, at least qualitatively. In contrast, the voltage independence of the 100 kHz, 1 MHz, and 10 MHz curves and the frequency dispersion of all of the $C-V$ curves are not expected. These anomalous trends are attributed to the presence of traps, as discussed in the following.

For a trap to contribute to the measured capacitance, both capture and emission of a carrier must occur quickly enough so that the trap is able to dynamically maintain a steady-state occupancy with respect to the measurement signal frequency.[21] Above a certain frequency for each trap, the trap can no longer follow the applied signal so that it no longer contributes to the measured capacitance.

In practice, trap emission usually establishes the steady-state trap occupancy. Assuming this to be the case, the critical trap depth, E_{trap}, beyond which traps can no longer maintain steady state with applied signal frequency f may be estimated from[21]

$$E_{\text{trap}} \approx k_B T \ln\left[\frac{\sigma_n v_{\text{th}} N_C}{2\pi f}\right], \tag{1}$$

where k_B is Boltzmann's constant, T is temperature, σ_n is the trap electron capture cross section, v_{th} is the electron thermal velocity, and N_C is the conduction-band density of states.

A decrease in the measured capacitance corresponds to an increase in the effective distance across which ac charge modulation occurs; the measurement signal frequency determines the critical energy depth of the traps that are able to contribute to the capacitance. Thus, the essential point is to recognize that a decrease in the measured capacitance can arise from a voltage-induced increase in the steady-state dc depletion region width, or as a consequence of a change in the measurement frequency due to the inability of traps to follow the measurement signal.

With these ideas in mind, consider Fig. 8, which displays the capacitance frequency dependence, with reverse voltage as a parameter. First, note that the frequency dependence is as strong or stronger than the voltage dependence. Thus, traps play an important role in establishing the capacitance trends shown in Fig. 8, as well as Fig. 7. Next, note that the voltage dependence is negligible above ~ 50 kHz, at a capacitance of ~ 30 nF/cm^2. This corresponds to the expected capacitance of the fully depleted i-ZnO layer. Thus, for frequencies above ~ 50 kHz, the $C-V$ curves shown in Fig. 7 are voltage independent because ac charge modulation occurs across the entire i-ZnO layer; traps within i-ZnO are no longer able to respond to the measurement signal frequency. Note that the reduction in capacitance with frequency for

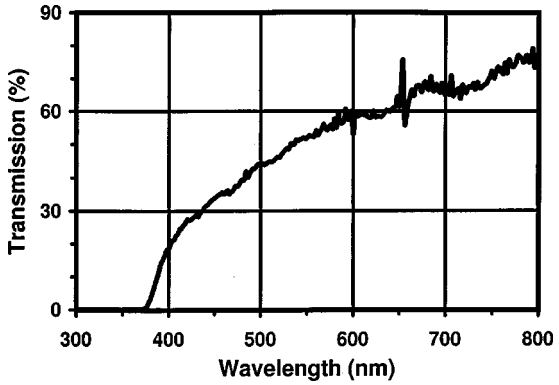

FIG. 9. Optical transmission spectrum of a $CuYO_2$:Ca (300 nm)/ZnO:Al (250 nm)/ITO (200 nm) $p-i-n$ heterojunction diode with a total thickness of 0.75 μm.

frequencies in excess of ~100 kHz is attributed to the diode RC time constant (i.e., a diode resistance of ~25 Ω and capacitance of ~2.5 nF result in a roll off of the measured capacitance beginning at ~100 kHz. In this assessment it is important to recognize that in the device R and C are in series, whereas the $C-f$ measurement is performed with the capacitance meter set to assume a parallel RC model; this results in a roll off in measured capacitance much earlier than expected from the RC time constant).

Using Eq. (1), the critical trap depths above which traps can no longer maintain steady-state with the applied signal frequency are estimated as ~0.3 and ~0.4 eV for frequencies of 50 and 1 kHz, respectively (assuming a neutral capture cross section of 10^{-15} cm^2). Thus, the traps responsible for the capacitance frequency dispersion evident in Figs. 7 and 8 are relatively shallow traps. Although these traps are relatively shallow, a Fermi-level position of 0.3–0.4 eV below the conduction-band minimum corresponds to a very small electron density in the *i*-ZnO of $\sim 10^{12}-10^{14}$ cm^{-3}. Thus, these trap depths are consistent with the semi-insulating nature of the *i*-ZnO layer.

As a conclusion to this section, notice that if the diode capacitance at 50 kHz is ~30 nF/cm^2 and corresponds to ac charge modulation across the full 250-nm-thick *i*-ZnO layer, this means that the effective widths corresponding to the 1 kHz diode capacitances of ~60–90 nF/cm^2, as shown in Fig. 8, are ~80–125 nm. Thus, ac charge modulation occurs a significant distance into the *i*-ZnO layer, and the traps giving rise to frequency dispersion of the capacitance originate in the *i*-ZnO bulk.

D. Optical transmission characteristics

For optical transmission measurements, the diode structure is fabricated under identical conditions on a glass/ITO substrate, but without use of the shadow mask for deposition of *p*-type $CuYO_2$:Ca. Figure 9 shows the optical transmission spectrum of a $CuYO_2$:Ca/ZnO:Al/ITO $p-i-n$ heterojunction diode with a total thickness of 0.75 μm. The optical transmission is ~35%–~65% in the visible region between 450 and 700 nm. This compares to an optical transmission in the visible of 20% reported by Sato et al. for their *p*–NiO/*i*-NiO/*i*-ZnO/*n*-ZnO $p-i-n$ heterojunction diode[6] and 70%–80% reported by Kudo *et al.* for their *p*-$SrCu_2O_2$/*n*-ZnO $p-n$ heterojunction diode.[6]

IV. CONCLUSIONS

All-oxide transparent n^+-ITO/*i*-ZnO/p^+-$CuYO_2$:Ca $p-i-n$ heterojunction diodes are fabricated and characterized. The diodes show rectifying current–voltage characteristics, dominated in forward bias by the flow of space-charge-limited current in the *i*-ZnO layer. Energy-band considerations indicate that band gap mismatch suppresses the injection of holes from the *p*-$CuYO_2$:Ca into the *i*-ZnO, so that the current–voltage characteristics differ from those of a typical $p-i-n$ homojunction diode. Capacitance measurements show a strong frequency dispersion, attributed to bulk traps in the *i*-ZnO layer.

ACKNOWLEDGMENTS

This work was funded by the National Science Foundation under Contract No. DMR-0071727 and by the Research Corporation.

[1] H. Kawazoe, M. Yasukawa, H. Hyodo, M. Kurita, H. Yanagi, and H. Hosono, Nature (London) **389**, 939 (1997).
[2] N. Duan, A. W. Sleight, M. K. Jayaraj, and J. Tate, Appl. Phys. Lett. **77**, 1325 (2000).
[3] M. K. Jayaraj, A. Draeseke, N. Duan, J. Tate, and A. W. Sleight, *Proceedings of the MRS Workshop on Transparent Conducting Oxides* (MRS, Denver, CO, 2000).
[4] K. Ueda, T. Hase, H. Yanagi, H. Kawazoe, H. Hosono, H. Ohta, M. Orita, and M. Hirano, J. Appl. Phys. **89**, 1790 (2001).
[5] R. Nagarajan, A. Draeseke, A. W. Sleight, and J. Tate, J. Appl. Phys. **89**, 8022 (2001).
[6] A. Kudo, H. Yanagi, K. Ueda, H. Hosono, H. Kawazoe, and Y. Yano, Appl. Phys. Lett. **75**, 2851 (1999).
[7] H. Ohta, K. Kawamura, M. Orita, M. Hirano, N. Sarukura, and H. Hosono, Appl. Phys. Lett. **77**, 475 (2000).
[8] H. Sato, T. Minami, S. Takata, and T. Yamada, Thin Solid Films **236**, 27 (1993).
[9] T. Aoki, Y. Hatanaka, and D. C. Look, Appl. Phys. Lett. **76**, 3257 (2000).
[10] H. Yanagi, T. Hase, S. Ibuki, K. Ueda, and H. Hosono, Appl. Phys. Lett. **78**, 1583 (2001).
[11] M. K. Jayaraj, A. D. Draeseke, J. Tate, R. L. Hoffman, and J. F. Wager, *Transport and Microstructural Phenomena in Oxide Electronics*, edited by D. S. Ginley, m. E. Hawley, D. C. Pain, D. H. Blank, and S. K. Streiffer (MRS, Denver, CO, 2001).
[12] T. Minami, T. Miyata, and T. Yamamoto, Surf. Coat. Technol. **108-109**, 583 (1998).
[13] V. Srikant and D. R. Clarke, J. Appl. Phys. **83**, 5447 (1998).
[14] F. A. Benko and F. P. Koffyberg, Can. J. Phys. **63**, 1306 (1985).
[15] H. Yanagi, S. Inoue, K. Ueda, H. Kawazoe, H. Hosono, and N. Hamada, J. Appl. Phys. **88**, 4159 (2000).
[16] L. F. Mattheiss, Phys. Rev. B **48**, 18300 (1993).
[17] R. J. Cava *et al.*, J. Solid State Chem. **104**, 437 (1993).
[18] F. A. Kröger, *The Chemistry of Imperfect Crystals*, 2nd ed. (North-Holland, Amsterdam, 1974).
[19] S. M. Sze, *Physics of Semiconductor Devices*, 2nd ed. (Wiley, New York, 1981).
[20] M. A. Lampert and P. Mark, *Current Injection in Solids* (Academic, New York, 1970).
[21] D. K. Schroder, *Semiconductor Material and Device Characterization*, 2nd ed. (Wiley, New York, 1998).